PHYSICAL REVIEW B VOLUME 49, NUMBER 13 1 APRIL 1994-I

Monte Carlo analysis of an interatomic potential for He

J. Boronat and J. Casulleras
Departament de Física i Enginyeria Nuclear, Universitat Politècnica de Catalunya, Pau Gargallo 5, E-08028 Barcelona, Spain

(Received 13 August 1993)

By means of a quadratic diffusion Monte Carlo method we have performed a comparative analysis between the Aziz potential and a revised version of it. The results demonstrate that the revised version produces a better description of the equation of state for liquid ^{4}He. In spite of the improvement in the description of derivative magnitudes of the energy, as the pressure or the compressibility, the energy per particle which comes from this revised potential is lower than the experimental one. The inclusion of three-body interactions, which give a repulsive contribution to the potential energy, makes it feasible that the calculated energy comes close to the experimental result.

I. INTRODUCTION

Many-body techniques have achieved a high level of accuracy in the description of atomic ^{3}He and ^{4}He, which constitute the most characteristic examples of quantum liquids. The theoretical approaches to the many-body problem can be classified in two large blocks depending on the use or nonuse of stochastic procedures. Among the nonstochastic methods it is the variational framework[1] combined with integral equations such as the hypernetted-chain (HNC), which has provided the best results for the ground state. Also, perturbation schemes constructed on [correlated basis (correlated basis function (CBF) theory[2]] has led one to extend this study to the lowest excited states. On the other hand, Monte Carlo (MC) methods[3] give exact information, within some statistical uncertainties, on the ground state of bosonic systems both at zero and finite temperature. The initial constraint imposed by the use of a finite number of particles in MC simulations does not influence appreciably to the energetic properties. However, the structure properties at $r \rightarrow \infty$ ($k \rightarrow 0$) related to long-range correlations are out of scope.

The high agreement between the theoretical results and the experimental data is also linked to the well-known interatomic interaction for He atoms (pairwise additive form). For the last ten years, the HFDHE2 potential proposed by Aziz *et al.*[4] has allowed for reproducing the energetic and structure properties of liquid He quite well both in homogeneous[5] and inhomogeneous phases.[6-8] Despite the accuracy of this pair potential a renewed version of it (HFD-B(HE)) was published by Aziz *et al.* in 1987.[9] The revised Aziz potential (hereafter referred to as Aziz II potential) was brought about as a consequence of several new theoretical and experimental results, which appeared in the literature between the publication of the two potentials. First, Ceperley and Partridge[10] pointed out by means of a quantum Monte Carlo calculation of the interaction energy of two He atoms, with internuclear separations less than 1.8 Å, that the Aziz potential is too repulsive below this distance. On the other hand, new experimental measurements of the second virial coefficients and transport properties for ^{3}He and ^{4}He showed evidence of some small inconsistencies of the Aziz potential. The explicit expressions of the Aziz and Aziz II potentials appear in Appendix A. Apart from a soft core, the Aziz II potential has its minimum at $\varepsilon = 10.95$ K, $r_m = 2.963$ Å, while Aziz potential has its minimum at $\varepsilon = 10.80$ K, $r_m = 2.967$ Å. Therefore, the new potential is only slightly deeper with the minimum localized at a lower interatomic separation.

To start on a theoretical comparative study between He potentials it is necessary to calculate the properties of the liquid as precisely as it is possible. Stochastic methods provide the appropriate tools for this purpose, especially in the case of bosonic systems as ^{4}He. In the past, the Green's function Monte Carlo method (GFMC) was used to elucidate between different models for the pair interaction. The main conclusion of this analysis[5] stated that the Aziz potential was the best interaction to study the properties of liquid and solid helium.

Our objective in the present work is to perform a comparative analysis between the two Aziz potentials to establish if the revised potential (Aziz II) produces even better results than the previous one. The calculation presented here follows an alternative procedure to GFMC known as diffusion Monte Carlo (DMC).

Both GFMC, developed by Kalos and co-workers,[11,12] and DMC algorithms[13,14] solve stochastically the Schrödinger equation in imaginary time. The GFMC scheme constructs a time-integrated Green's function by means of a double Monte Carlo sampling. On the other hand, the DMC algorithm is a simpler method that assumes an approximate form for the Green's function for small time steps Δt. In this case, after an iterative process and sufficiently long times, only the ground-state wave function survives. Therefore, the exact energy per particle of the system is obtained when the limit $\Delta t \rightarrow 0$ is considered. DMC is posterior to GFMC, but up to now it has already been applied to the study of small molecules,[14] solid hydrogen,[15] or ^{4}He clusters.[7] The main disadvantage of the DMC algorithms used in the major part of those works is that the energy eigenvalues change linearly with Δt. This fact obliges one to perform several calculations using different values for the time step and next to extrapolate the exact value in the limit $\Delta t \rightarrow 0$. To avoid this difficulty several quadratic algorithms have been devised, but the success of this improvement has not been complete. Recently, a new quadratic diffusion Monte Carlo (QDMC) method[16] has proved to work efficiently in the description of ^{4}He droplets.[7] In the present work, we use a QDMC method with a very similar algorithm to the one reported in Ref. 16. In the next sections of the article we will justify the accuracy of the proposed method, which allows for the possibility of calculating the properties of the system at a finite time-step without introducing any significant difference with the extrapolated value.

The outline of this paper is as follows: In Sec. II the quadratic diffusion Monte Carlo method to solve the Schrödinger equation is presented. The consistency of the algorithm is checked by using different trial functions and several numbers of particles. The time-step dependence of the energy per particle shows the expected quadratic behavior. A comparative analysis of the two Aziz potentials is reported in Sec. III. A perturbative estimation of the contributions coming from various three-body potentials is also reported. A brief discussion and conclusions comprise Sec. IV.

II. COMPUTATIONAL ALGORITHM

The starting point in diffusion Monte Carlo methods is the Schrödinger equation for N particles written in imaginary time:

$$-\frac{\partial\Psi(\mathbf{R},t)}{\partial t}=(H-E)\Psi(\mathbf{R},t)\ , \tag{1}$$

where $\mathbf{R}\equiv(\mathbf{r}_1,\ldots,\mathbf{r}_N)$ and t is measured in units of $\hbar$. $\Psi(\mathbf{R},t)$ can be expanded in terms of a complete set of eigenfunctions $\phi_i(\mathbf{R})$ of the Hamiltonian:

$$\Psi(\mathbf{R},t)=\sum_n c_n \exp[-(E_i-E)t]\phi_i(\mathbf{R})\ , \tag{2}$$

where E_i is the eigenvalue associated to $\phi_i(\mathbf{R})$. The asymptotic solution of Eq. (1) for any value E close to the energy of the ground state and for long times ($t\to\infty$) gives $\phi_0(\mathbf{R})$, provided that there is a nonzero overlap between $\Psi(\mathbf{R},t=0)$ and the ground-state wave function $\phi_0(\mathbf{R})$.

In a computer simulation of Eq. (1) it is crucial to use the importance sampling technique[12] in order to reduce the statistical fluctuations to a manageable level. Following this method, one rewrites the Schrödinger equation for the function:

$$f(\mathbf{R},t)\equiv\psi(\mathbf{R})\Psi(\mathbf{R},t)\ , \tag{3}$$

where $\psi(\mathbf{R})$ is a time-independent trial function. Consider a Hamiltonian of the form

$$H=-\frac{\hbar^2}{2m}\nabla_R^2+V(\mathbf{R})\ , \tag{4}$$

Eq. (1) turns out to be

$$\begin{aligned}-\frac{\partial f(\mathbf{R},t)}{\partial t}&=-D\nabla_R^2 f(\mathbf{R},t)+D\nabla_{\mathbf{R}}(\mathbf{F}(\mathbf{R})f(\mathbf{R},t))\\&\quad+[E_L(\mathbf{R})-E]f(\mathbf{R},t)\\&\equiv(A_1+A_2+A_3)f(\mathbf{R},t)\equiv Af(\mathbf{R},t)\ ,\end{aligned} \tag{5}$$

where $D=\hbar^2/(2m)$, $E_L(\mathbf{R})=\psi(\mathbf{R})^{-1}H\psi(\mathbf{R})$ is the local energy, and

$$\mathbf{F}(\mathbf{R})=2\psi(\mathbf{R})^{-1}\nabla_{\mathbf{R}}\psi(\mathbf{R}) \tag{6}$$

is called the drift force. $\mathbf{F}(\mathbf{R})$ acts as an external force which guides the diffusion process, involved by the first term in Eq. (5), to regions where $\psi(\mathbf{R})$ is large.

The formal solution of Eq. (5) is

$$f(\mathbf{R}',t+\Delta t)=\int G(\mathbf{R}',\mathbf{R},\Delta t)f(\mathbf{R},t)d\mathbf{R} \tag{7}$$

with

$$G(\mathbf{R}',\mathbf{R},\Delta t)=\langle\mathbf{R}'|\exp(-A\Delta t)|\mathbf{R}\rangle\ . \tag{8}$$

While GFMC method works with the whole Green's function, DMC algorithms rely on reasonable approximations of $G(\mathbf{R}',\mathbf{R},\Delta t)$ for small values of the time step Δt. Then, Eq. (8) is not directly solved but iterated repeatedly to obtain the asymptotic solution $f(\mathbf{R},t\to\infty)$.

In the quadratic diffusion Monte Carlo algorithm we have used, the Green's function $G(\mathbf{R}',\mathbf{R},\Delta t)$ is approximated by

$$\exp(-A\Delta t)=\exp\left[-A_3\frac{\Delta t}{2}\right]\exp\left[-A_2\frac{\Delta t}{2}\right]\exp(-A_1\Delta t)\exp\left[-A_2\frac{\Delta t}{2}\right]\exp\left[-A_3\frac{\Delta t}{2}\right]\ . \tag{9}$$

This decomposition, which is not unique,[16] is exact up to order $(\Delta t)^2$. Assuming (9), Eq. (7) becomes

$$\begin{aligned}f(\mathbf{R}',t+\Delta t)=\int\Bigg[&G_3\left[\mathbf{R}',\mathbf{R}_1,\frac{\Delta t}{2}\right]G_2\left[\mathbf{R}_1,\mathbf{R}_2,\frac{\Delta t}{2}\right]G_1(\mathbf{R}_2,\mathbf{R}_3,\Delta t)\\&\times G_2\left[\mathbf{R}_3,\mathbf{R}_4,\frac{\Delta t}{2}\right]G_3\left[\mathbf{R}_4,\mathbf{R},\frac{\Delta t}{2}\right]\Bigg]f(\mathbf{R},t)d\mathbf{R}_1\cdots d\mathbf{R}_4 d\mathbf{R}\ ,\end{aligned} \tag{10}$$

with

$$G_1(\mathbf{R}',\mathbf{R},t)=(4\pi Dt)^{-3N/2}\exp\left[-\frac{(\mathbf{R}'-\mathbf{R})^2}{4Dt}\right]\ , \tag{11}$$

$$G_2(\mathbf{R}',\mathbf{R},t)=\delta(\mathbf{R}'-\mathbf{R}(t)), \quad \text{where} \begin{cases} \mathbf{R}(0)=\mathbf{R} \\ \dfrac{d\mathbf{R}(t)}{dt}=D\mathbf{F}(\mathbf{R}(t)) \, , \end{cases} \tag{12}$$

and

$$G_3(\mathbf{R}',\mathbf{R},t)=\exp[-(E_L(\mathbf{R})-E)t]\delta(\mathbf{R}'-\mathbf{R}) \, . \tag{13}$$

In our Monte Carlo computations, $f(\mathbf{R},t)$ is represented by n_w walkers $\mathbf{R}_i$, each one representing a set of the $3N$ coordinates of the N particles. The algorithm used for the implementation of Eq. (10) goes through the following steps.

(1) Move the walkers, under the drift force $\mathbf{F}(\mathbf{R})$, during an interval $\Delta t/2$ with accuracy $(\Delta t)^2$.

(2) Apply to each walker a displacement χ randomly drawn from the $3N$ Gaussian distribution $\exp[-\chi^2/(4D\Delta t)]$.

(3) Repeat step (1).

(4) Randomly replicate each walker n_r times, in such a way that

$$\langle n_r \rangle = \exp\left[-\Delta t\left[\frac{E_L(\mathbf{R}')+E_L(\mathbf{R})}{2}-E\right]\right] \, .$$

(5) Go to step (1) for the next walker $\mathbf{R}_i$, until the set of walkers is exhausted. The new set obtained corresponds to $f(\mathbf{R},t+\Delta t)$.

The whole procedure is repeated as many times as is needed to reach the asymptotic limit ($t \rightarrow \infty$). From then on, the walkers $\mathbf{R}_i$ are used to obtain the expectation values of the magnitudes to be determined.

In order to establish the preciseness of the method several aspects have to be considered. First, the mixed estimator for the expectation value of an operator A, i.e., $\langle \psi | A | \Psi \rangle$, only gives the exact result when A commutes with the Hamiltonian. To obtain the expectation value of an operator, which does not commute with H, we can use a linear extrapolation[11]

$$\langle \Psi | A | \Psi \rangle = 2\langle \psi | A | \Psi \rangle - \langle \psi | A | \psi \rangle \, . \tag{14}$$

This simple perturbative method involves the performance of a variational Monte Carlo (VMC) calculation to determine the variational expectation value $\langle \psi | A | \psi \rangle$. It is interesting to notice that a VMC calculation can be carried out with the same algorithm described for DMC only suppressing the branching term (13).

In Table I, the results for the potential, kinetic and total energies per particle obtained with VMC and QDMC methods are shown together with a GFMC result.[5] They correspond to an Aziz potential calculation with $N=128$ at density $\rho=0.365\sigma^{-3}$ ($\sigma=2.556$ Å). The trial wave functions ψ_{J_1} and ψ_{J_2} contain different two-body correlation factors, and ψ_{JT} includes also three-body correlations. Explicit expressions of these trial functions, together with the values of the parameters involved in them, are given in Appendix B.

As it is shown in Table I, there are not significative discrepancies between the QDMC results for the total energy. The perfect agreement between the QDMC results and the GFMC value is also remarkable. Equation (14) is used to estimate the kinetic and potential contributions to the total energy. In spite of its simplicity, this method gives very similar values for the partial energies even when trial wave functions as different as the ones reported in Table I are used as importance sampling. New methods to avoid the slight influence of the trial wave function in the extrapolated estimators have been recently suggested by Barnett, Reynolds, and Lester[17] and Zhang and Kalos.[18]

The effect of a finite volume simulation box has also been considered, raising the number of particles N from $N=128$ (which has been used for the bulk of the calculation) up to $N=190$ for ψ_{J2} and $\rho=0.365\ \sigma^{-3}$. The differences encountered were compatible with the size of the statistical fluctuations reported in Table I.

Another important parameter in the calculation is the population of walkers n_w. All the results reported in the present work have been obtained after a preliminary analysis of the influence of the population in the average energy of the system, and the final results correspond to

TABLE I. Results for the total, kinetic and potential energies for different trial wave functions. The forms of ψ_{J1}, ψ_{J2}, nd ψ_{JT}, as well as the values of the parameters entering into them, are noted explicitly in Appendix B. In the last row, the GFMC results from Refs. 5 and 27 are also reported. All energies are in degrees kelvin per particle.

	E/N	T/N	V/N
VMC ψ_{J1}	-5.683 ± 0.014	15.119 ± 0.005	-20.802 ± 0.009
VMC ψ_{J2}	-5.881 ± 0.005	15.248 ± 0.004	-21.129 ± 0.007
VMC ψ_{JT}	-6.617 ± 0.007	14.552 ± 0.030	-21.169 ± 0.018
QDMC ψ_{J1}	-7.115 ± 0.010	14.589 ± 0.020	-21.704 ± 0.020
QDMC ψ_{J2}	-7.121 ± 0.010	14.576 ± 0.025	-21.697 ± 0.023
QDMC ψ_{JT}	-7.125 ± 0.005	14.417 ± 0.030	-21.542 ± 0.020
GFMC	-7.120 ± 0.024[a]	14.47 ± 0.09[b]	-21.59 ± 0.09[b]

[a] Reference 5.

[b] Reference 27.

the empirical asymptotic value of n_w. This asymptotic population decreases when one improves the quality of the trial wave function ψ. In fact, whereas $n_w=400$ for ψ_{J1} and ψ_{J2} this value is reduced to $n_w=250$ in the ψ_{JT} case. Actually, we have developed a parallel QDMC code based on the equal role played by the different walkers. The calculation has been carried out on a massively parallel computer *CM*2, which best performance is obtained when a large number of walkers is considered. The length of the series have been 12 000–15 000 for ψ_{J1} and ψ_{J2} and 8000–10 000 for ψ_{JT}.

A final but not less important point is the time-step dependence of the QDMC algorithm. In Fig. 1 it is shown a characteristic result of the total energy as a function of the time step Δt. The time t is measured in reduced units τ, where

$$\tau=\frac{m\sigma^2}{2\hbar} . \tag{15}$$

As one can see in the figure, there is a clear departure from the linear time dependence supplied by the linear DMC algorithms. If a second-order polynomial fit $E/N=(E/N)_0+A(\Delta t)^2$ (solid line in the figure) to the QDMC results is performed, one obtains an extrapolated value of $(E/N)_0=(-7.124\pm0.003)$ K, which is indistinguishable from the values obtained working with $\Delta t=(1-2)\times10^{-3}\tau$. Therefore, it is plausible to calculate the properties of the system accurately using a single value for Δt, lying in the stated range, without the necessity of a complete analysis in time to extrapolate the correct results.

III. RESULTS

In this section the numerical results for the energy and for the structure properties using the Aziz and Aziz II potentials are presented. First, we analyze the differences between the two interatomic potentials and then, the contribution to the total energy of several models for the three-body interactions. In all the calculations reported below the trial function ψ_{J2} (see Appendix B) has been used as importance sampling. The average population size (n_w) ranges from 400, near the equilibrium density ($\rho=0.365\sigma^{-3}$), to 900 for the highest densities. On the other hand, the value for the time step has been taken as $\Delta t=1.25\times10^{-3}\tau$ around the equilibrium density and $\Delta t=1.0\times10^{-3}\tau$ for higher densities. No significant deviations in the results of the energy are observed when these Δt values are doubled.

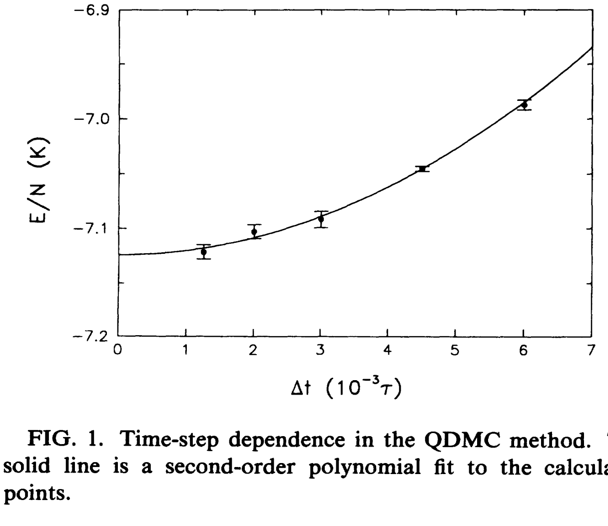

FIG. 1. Time-step dependence in the QDMC method. The solid line is a second-order polynomial fit to the calculated points.

A. Two-body potentials: Aziz vs Aziz II

As it has been commented in the Introduction, the differences between the Aziz and Aziz II potentials are not very large. However, slight differences in the values of the parameters entering into $V(r)$ produce relatively large changes in the energy as it was asserted by Kalos *et al.*[5] in their GFMC calculation of the equation of state of liquid ^{4}He using the Aziz potential. The energies obtained for both potentials, together with the experimental results of Ref. 19 are reported in Table II. In parenthesis there are the GFMC results[5] for the Aziz potential. The GFMC and QDMC calculations are in good agreement, but a small deviation between both results is obtained at high densities. The kinetic and potential energies are also given in the table. The potential energy has been calculated by means of the extrapolated estimator [Eq. (14)], and the kinetic energy comes from the difference between the total and the potential energies. A comparison between the partial energies of the two potentials reveals that, while the kinetic energy is practically the same, the Aziz II potential energy is, in absolute value, larger than the Aziz one. In particular, the Aziz II potential lowers the potential energy with respect to the Aziz case in a quantity, which grows from ~0.19 K at $\rho=0.365\ \sigma^{-3}$ to ~0.23 K at the highest density $\rho=0.490\ \sigma^{-3}$. The partial energies for both potentials satisfy the lower bound for the kinetic energy and the upper bound for the potential energy ($T/N\geq13.4$ K and $V/N\leq-20.6$ K, at the equilibrium density).[20]

Concerning the total energies, one can observe that the experimental values are approximately located at the middle of the Aziz and Aziz II results. This fact is clear from Fig. 2, where the equation of state of liquid ^{4}He is shown in comparison with the experimental results. The lines in the figure correspond to numerical fits to the results reported in Table II, excluding the highest density (0.490 σ^{-3}) because it is quite far from the experimental freezing density $\rho_l=0.430\ \sigma^{-3}$. In the majority of microscopic calculations on liquid He a polynomial fit of the form

$$e=e_0+B\left[\frac{\rho-\rho_0}{\rho_0}\right]^2+C\left[\frac{\rho-\rho_0}{\rho_0}\right]^3 , \tag{16}$$

where $e=E/N$ and ρ_0 is the equilibrium density, has been used to determine the equation of state. On the other hand, in calculations based on density functional theory the form

$$e=b\rho+c\rho^{1+\gamma} , \tag{17}$$

proposed by Stringari and Treiner,[21] has proved to be very efficient in describing properties of homogeneous and inhomogeneous [including an additional surface term

TABLE II. Results for the total and partial energies from the QDMC calculations with the Aziz potential, the Aziz II potential, and experiment (Ref. 19). The numbers quoted in parentheses are taken from Ref. 5. All energies are in degrees kelvin per particle.

	Aziz			Aziz II			Expt.
$\rho(\sigma^{-3})$	E/N	T/N	V/N	E/N	T/N	V/N	E/N
0.328	-6.988 ± 0.013 (-7.034 ± 0.037)	12.107 ± 0.018	-19.095 ± 0.013	-7.150 ± 0.010	12.152 ± 0.032	-19.302 ± 0.030	
0.365	-7.121 ± 0.010 (-7.120 ± 0.024)	14.576 ± 0.025	-21.697 ± 0.023	-7.267 ± 0.013	14.622 ± 0.027	-21.889 ± 0.024	-7.17
0.401	-6.892 ± 0.013 (-6.894 ± 0.048)	17.262 ± 0.030	-24.154 ± 0.027	-7.150 ± 0.016	17.302 ± 0.038	-24.452 ± 0.035	-7.03
0.424	-6.696 ± 0.024	19.152 ± 0.042	-25.848 ± 0.035	-6.877 ± 0.022	19.218 ± 0.037	-26.095 ± 0.030	-6.77
0.438	-6.422 ± 0.020 (-6.564 ± 0.058)	20.447 ± 0.036	-26.869 ± 0.030	-6.660 ± 0.017	20.398 ± 0.034	-27.058 ± 0.030	-6.55
0.490	-5.010 ± 0.025 (-5.175 ± 0.101)	25.402 ± 0.047	-30.412 ± 0.040	-5.222 ± 0.025	25.404 ± 0.050	-30.626 ± 0.043	

in Eq. (17)] liquid ^{4}He. In the case of the Aziz II potential both analytic forms are compatible with the results of the energy, taking into account their respective errors. However, we have checked that only the function (17) provides the correct result for the energy when densities lower than $0.328\sigma^{-3}$ are considered. Therefore, all the results presented below, concerning the equation of state, are derived starting on the second option [Eq. (17)].

The values of the parameters which best fit our Aziz II potential results are

$$\begin{aligned} b &= (-27.258\pm0.017)K\sigma^3 , \\ c &= (114.95\pm0.22)K\sigma^{3(1+\gamma)} , \\ \gamma &= 2.7324\pm0.0020 . \end{aligned} \tag{18}$$

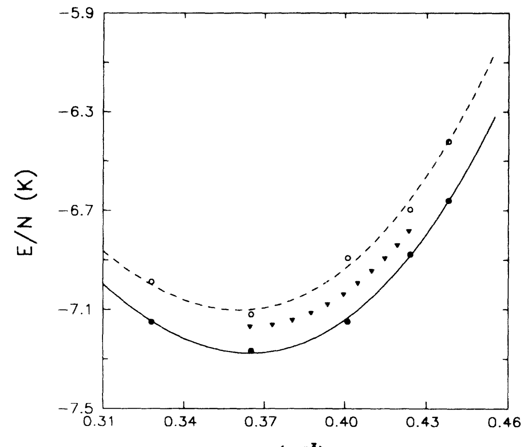

FIG. 2. Equation of state for liquid ^{4}He. The circles are the QDMC results with the Aziz potential and the dashed line is a fit to the calculated energies. The solid circles correspond to the QDMC energies with the Aziz II potential; the solid line is a fit to these energies. These fits have been performed with Eq. (17), the parameters being those given in (18) and (19) for the Aziz II and Aziz potentials, respectively. The experimental values, represented by solid triangles, are taken from Ref. 19. The error bars of the QDMC results are smaller than the size of the symbols.

The same analysis has been performed by taking the energy results of the Aziz potential. In this case, neither the polynomial form (16) nor Stringari's (17) are statistically compatible with our results. This fact is clearly reflected in Fig. 2, where several Aziz points (the size of each point is larger than its error bar) are not intersected by the result of the fit (represented with a dashed line). In spite of this severe restriction, and to make possible the comparison with the equation of state provided by the Aziz II potential, the optimum values

$$\begin{aligned} b &= (-26.947\pm0.016)K\sigma^3 , \\ c &= (115.72\pm0.21)K\sigma^{3(1+\gamma)} , \\ \gamma &= 2.7160\pm0.0020 \end{aligned} \tag{19}$$

are taken.

We have also fitted the same type of function to the experimental results of Ref. 19. In this case, the parameters b and c have been fixed to reproduce the equilibrium density and the energy at this density, whereas the parameter γ has been obtained by means of a numerical fit to all the energies reported in that work. The values obtained are

$$\begin{aligned} b &= -26.746K\sigma^3 , \\ c &= 116.69K\sigma^{3(1+\gamma)} , \\ \gamma &= 2.7773 . \end{aligned} \tag{20}$$

Once the equation of state $e(\rho)$ is known, it is straightforward to calculate the isothermal compressibility, defined as

$$\kappa(\rho)=\frac{1}{\rho}\left[\frac{\partial\rho}{\partial P}\right]_T , \tag{21}$$

where $P(\rho)=\rho^2(\partial e/\partial\rho)$ is the pressure, and the velocity of sound given by

$$c(\rho)=\left[\frac{1}{m\kappa\rho}\right]^{1/2} . \tag{22}$$

In Table III the results of the pressure, the compressibility and the velocity of sound of the two Aziz potentials are compared with the corresponding experimental

TABLE III. QDMC results for the pressure P, the compressibility κ and the velocity of sound c at the experimental equilibrium density using the Aziz and Aziz II potentials. The last row contains the experimental values derived from the experimental equation of state (20).

	P (atm)	κ (atm^{-1})	c (m/s)
Aziz	0.878±0.073	0.01199±0.00004	241.53±0.44
Aziz II	−0.019±0.075	0.01241±0.00004	237.40±0.46
Expt.	0	0.0124	237.2

values at the experimental equilibrium density ($\rho_0^{\text{expt}}=0.3646\sigma^{-3}$). The accuracy provided by the Aziz II potential is remarkable, giving results for these quantities which are indistinguishable from the experiment. Conversely, the equation of state corresponding to the Aziz potential supplies results which are slightly worse. The differences between the equations of state for the two potentials remain when the density increases, as one can see for $P(\rho)$ in Fig. 3 and for $\kappa(\rho)$ in Fig. 4. The equation of state corresponding to the Aziz II potential gives an excellent description of these magnitudes for all the values of the density here considered.

Apart from the ground-state energy, the Monte Carlo methods yield other interesting information. The radial distribution function

$$g(r_{12})=\frac{N(N-1)}{\rho^2}\frac{\int |\Psi(\mathbf{r}_1,\ldots,\mathbf{r}_N)|^2 d\mathbf{r}_3\cdots d\mathbf{r}_N}{\int |\Psi(\mathbf{r}_1,\ldots,\mathbf{r}_N)|^2 d\mathbf{r}_1\cdots d\mathbf{r}_N} \tag{23}$$

and its Fourier transform, the static structure function

$$S(k)=1+\rho\int d\mathbf{r}\, e^{i\mathbf{k}\cdot\mathbf{r}}[g(r)-1] \tag{24}$$

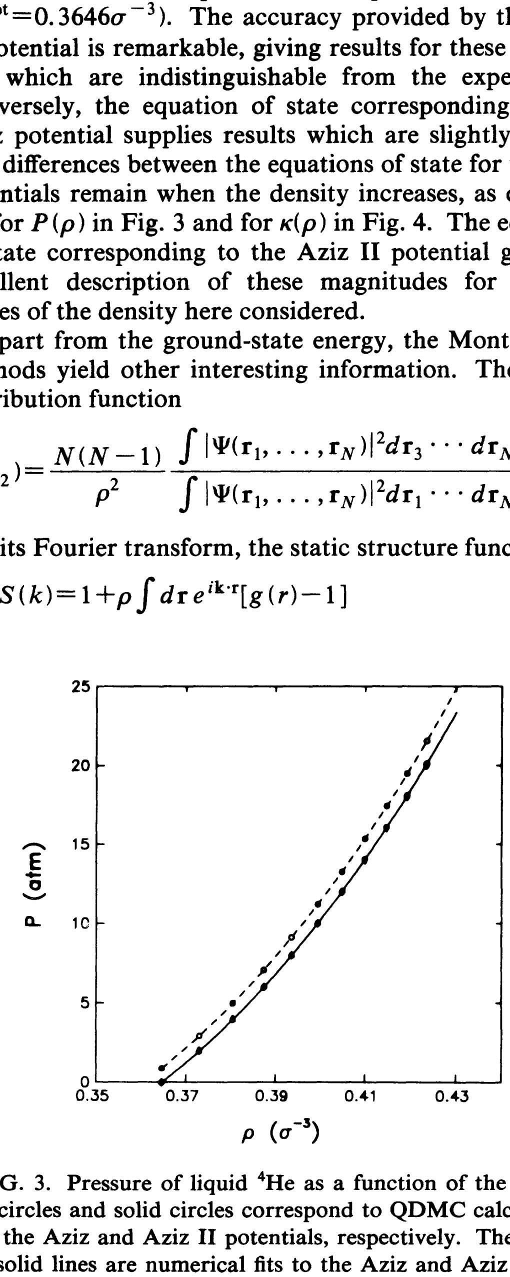

FIG. 3. Pressure of liquid ^{4}He as a function of the density. The circles and solid circles correspond to QDMC calculations with the Aziz and Aziz II potentials, respectively. The dashed and solid lines are numerical fits to the Aziz and Aziz II pressures, respectively. The experimental results, from the experimental equation of state (20), are represented by diamonds, which are practically hidden below the Aziz II values. The error bars of the QDMC results are smaller than the size of the symbols.

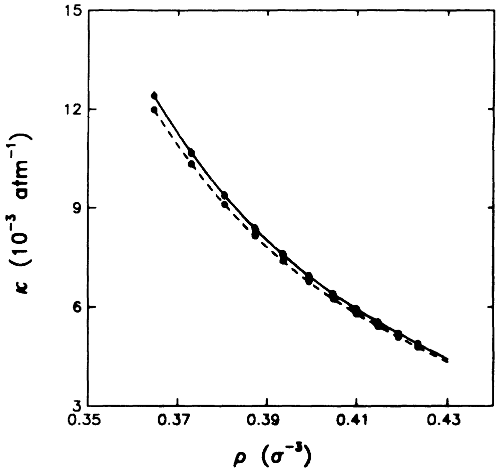

FIG. 4. Isothermal compressibility of liquid ^{4}He as a function of the density. The same notation as in Fig. 3.

are fundamental in the study of fluids. The calculation of these quantities is more involved than the calculation of the energy,[11,22] but the extrapolation procedure [Eq. (14)] allows results which are practically independent of the trial function used as importance sampling.

The radial distribution function $g(r)$, obtained in an Aziz II calculation at a density $\rho=0.365\sigma^{-3}$, is shown in Fig. 5 in comparison with an experimental determination at $T=1.0$ K by Svensson *et al.*[23] There is a good agreement between the calculated and the experimental $g(r)$, mainly in the first peak. In Fig. 6, the structure function $S(k)$, obtained by means of a Fourier transform of the $g(r)$ shown in Fig. 5, is plotted together with the experimental measure of Ref. 23. Due to the finite size of the simulation box, there are not reliable results for $S(k)$ for $k \lesssim 1$ Å^{-1}. The theoretical $S(k)$ is again very close to the experimental result, but the height of the experimental main peak is slightly higher. On the other hand, other

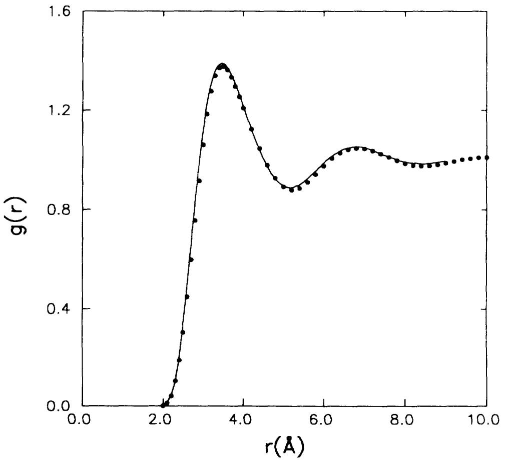

FIG. 5. Two-body radial distribution function at the experimental equilibrium density. The solid line is the QDMC result and the solid circles correspond to the neutron diffraction experimental determination from Ref. 23.

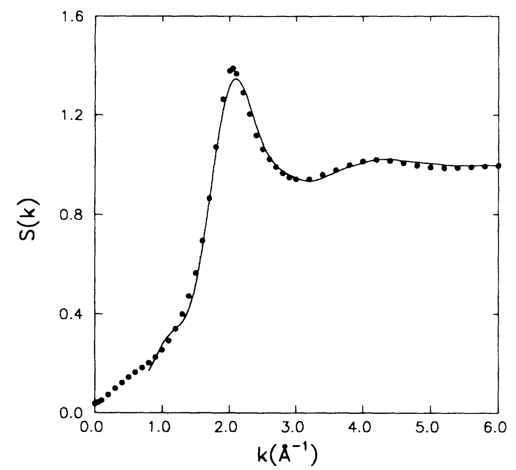

FIG. 6. Static structure function at the experimental equilibrium density. The solid line is the QDMC result, obtained by a Fourier transform of the radial distribution function showed in Fig. 5. The solid circles are the experimental determination from Ref. 23.

experimental determinations of $S(k)$ (Ref. 24) point to lower values of the intensity of the first peak, even below our results. In fact, analysis of the influence of the temperature T in $S(k)$ (Refs. 24 and 25) indicate that the largest variation of the structure function with T is placed in the vicinity of the first peak.

The one-body density matrix $\rho(r)$ defined as

$$\rho(r_{11'})=N\frac{\int \Psi(\mathbf{r}_1',\ldots,\mathbf{r}_N)\Psi(\mathbf{r}_1,\ldots,\mathbf{r}_N)d\mathbf{r}_2\cdots d\mathbf{r}_N}{\int |\Psi(\mathbf{r}_1,\ldots,\mathbf{r}_N)|^2 d\mathbf{r}_1\cdots d\mathbf{r}_N} \tag{25}$$

and its Fourier transform, the momentum distribution

$$n(k)=(2\pi)^3\rho n_0\delta(\mathbf{k})+\rho\int d\mathbf{r}\, e^{i\mathbf{k}\cdot\mathbf{r}}[\rho(r)-\rho(\infty)] \tag{26}$$

can also be computed using the configurations generated by the QDMC code. The function $\rho(r)$ is obtained as the expectation value of the operator

$$\left\langle \frac{\Psi(\mathbf{r}_1,\ldots,\mathbf{r}_i+\mathbf{r},\ldots,\mathbf{r}_N)}{\Psi(\mathbf{r}_1,\ldots,\mathbf{r}_N)} \right\rangle \tag{27}$$

evaluated on the configuration space over a set of random displacements of the particle i. The condensate fraction n_0, i.e., the fraction of particles occupying the zero momentum state, may be extracted from $\rho(r)$ by means of the asymptotic condition

$$n_0=\lim_{r\to\infty}\rho(r)\ . \tag{28}$$

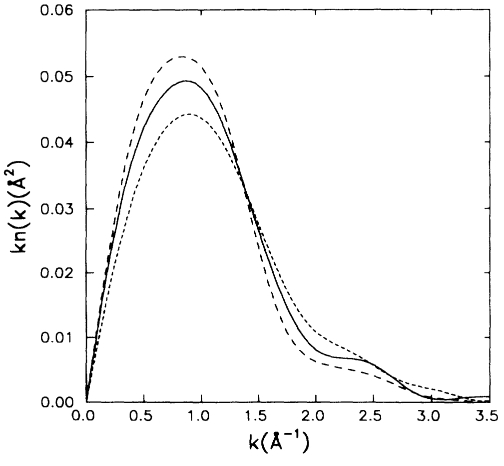

FIG. 7. Dependence of the calculated momentum distribution on density. The long-dashed, solid, and short-dashed lines stand for the results at densities of $0.328\sigma^{-3}$, $0.365\sigma^{-3}$, and $0.401\sigma^{-3}$, respectively.

In Fig. 7 the momentum distribution obtained via Eq. (26) is plotted, as $kn(k)$, for three values of the density. The correlations between the particles make the population of states with high momenta increase with the density. The shoulder observed at $k\simeq 2$ Å^{-1} for the three curves, which has been observed in other theoretical calculations of $n(k)$,[26,27] has been attributed in the past to the zero-point motion of the rotons.[28] On the other hand, it has been proved that if the condensate fraction is nonzero, $n(k)$ diverges as $1/k$ when $k\to 0$.[29] Again, the finite value of the simulation cell precludes the possibility of reproducing this behavior.

We have also determined the condensate fraction from the extrapolated estimation of $\rho(r)$ and the relation (28). At the equilibrium density, we get $n_0=0.084\pm0.001$, which is a value slightly smaller than the one obtained in a GFMC calculation (0.092 ± 0.001) (Ref. 27) using the Aziz potential. The discrepancy between the two results are not due to the use of different potentials. In fact, we have calculated $\rho(r)$ for the two Aziz potentials and no significant differences appear. The same conclusion holds for the radial distribution function $g(r)$.

A final point of interest is the density dependence of the condensate fraction. In Fig. 8, the change in the value of n_0 is shown for a wide range of densities. The condensate fraction decreases with the density, following a law nearly quadratic in ρ. In the figure, a quadratic fit to the results is shown as a "guide to the eye."

B. Three-body interactions

The importance of three-body interactions in helium has been discussed for a long time. It has been argued that these interactions would be present in He but its relative contribution to the total energy is still open to question. The most widely known model for the three-body potential is the triple-dipole interaction derived by Axilrod and Teller[30] considering perturbative theory. The Axilrod-Teller (AT) potential, which has been usually considered as the major contribution to the energy coming from the three-body interactions, provides a positive correction to the potential energy. The amount of this effect was calculated for the first time by Murphy and Barker[31] by means of a variational Monte Carlo calculation. Afterwards, that contribution was estimated by Kalos and co-workers[5,22] in a Rayleigh-Schrödinger perturbative calculation starting on GFMC configurations. From this analysis it was pointed out that, on the one

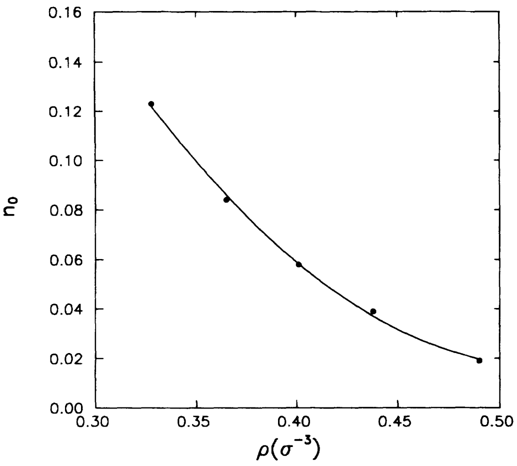

FIG. 8. Condensate fraction in liquid ^{4}He as a function of density. The solid line is a second-order polynomial fit to the calculated values. The error bars of the results are smaller than the size of the symbols.

hand, the GFMC prediction for the expectation value of the three-body potential $\langle V_3 \rangle$ was in accordance with the variational results of Murphy and Barker and, on the other, there were no relevant differences between the results coming from a Lennard-Jones and an Aziz potential calculations. Another conclusion of these GFMC works was that the inclusion of three-body potential contributions on the total energy worsened the two-body results along the whole equation of state.

In spite of the AT potential being the dominant contribution to $\langle V_3 \rangle$, it has been proved that at short interparticle separations a nonadditive and attractive force emerges. This short-ranged three-body interaction, usually known as exchange interaction, is due to the influence in the charge densities of two interacting atoms by the presence of a third near particle. Bruch and McGee (BM)[32] proposed a model potential to account for this effect, fitting the parameters of the exchange part to the atomic calculations of the energy of three He atoms at very short distances from Novaro and Beltran-Lopez.[33] Loubeyre[34] has proved that the BM three-body potential, in conjunction with the Aziz potential, accurately describes solid helium at high pressures and room temperature. The explicit forms for the AT and BM potentials are given in Appendix A.

As has been previously discussed, the Aziz II results for the energy per particle are below the experimental results for all the densities considered (see Fig. 2). Therefore, the inclusion of a repulsive contribution to the potential energy, arising from three-body interactions, could bring the theoretical results nearer to the experimental ones. In Table IV the results for the total (E/N) and potential (V/N) energies are reported in comparison with the experimental values of the energy. In all cases, the three-body potential energy is obtained by means of a Rayleigh-Schrödinger perturbation calculation, following the method described by Whitlock *et al.*[22] As one can see, the AT potential produces an increase in the energy, leading to values which are slightly higher than the experiment. Moreover, the difference between the Aziz II+AT and experimental values increases appreciably with the density, yielding to poor results for derivative magnitudes of the energy as the pressure or the compressibility. The results of the energy, using the BM potential, appear in the second column of Table IV. The exchange part of the BM potential practically cancels the repulsive contribution of the dispersion term (AT) becoming even dominant at the highest densities. The resulting energies lie very near to the two-body calculation but also in this case, as in the AT one, with a worsening reproduction of the dependence of the energy with the density. Therefore, neither the simple AT potential nor the more elaborated one (BM) improve, in a significant way, the Aziz II results. In fact, it seems more convincing that, in the density regime of liquid ^{4}He, the main three-body contribution comes from the AT potential, the exchange part of the BM potential being too large. We should notice that the parameters of the BM potential have been fitted to reproduce the energy of helium trimers with interparticle separations considerably less than the characteristic mean distance between the atoms in the liquid. Then, it is uncertain that the same parameters, or even the same analytical form, could be used to study the liquid phase.

In the third column of Table IV, labeled as MBM, we report the results which are obtained by using the BM potential with a modified value $A' = A/3$ (see Appendix A). Now, the energy at the experimental equilibrium density reproduces the experimental result and a quite

TABLE IV. Energies from the QDMC calculations with the Aziz II potential including the perturbative estimation of the expectation value of several models for the three-body interactions (AT, BM, and MBM; see text). The last column contains the experimental values. All energies are in degrees kelvin per particle.

	Aziz II+AT		Aziz II+BM		Aziz II+MBM		Expt.
$\rho(\sigma^{-3})$	E/N	V/N	E/N	V/N	E/N	V/N	E/N
0.328	−7.045	−19.197	−7.122	−19.274	−7.071	−19.223	
0.365	−7.127	−21.749	−7.249	−21.871	−7.168	−21.790	−7.17
0.401	−6.971	−24.273	−7.141	−24.443	−7.027	−24.329	−7.03
0.424	−6.668	−25.886	−6.886	−26.104	−6.741	−25.959	−6.77
0.438	−6.435	−26.833	−6.675	−27.073	−6.515	−26.913	−6.55
0.490	−4.913	−30.317	−5.323	−30.727	−5.050	−30.454	

good description is also obtained at higher densities. In Fig. 9, the equation of state obtained with the Aziz II-MBM model is depicted together with the experimental and the Aziz II results. The values of the parameters of the fit for the Aziz II+MBM calculation are

$$\begin{aligned} b &= (-27.202\pm0.017)K\sigma^3 , \\ c &= (114.11\pm0.21)K\sigma^{3(1+\gamma)} , \\ \gamma &= 2.6961\pm0.0020 . \end{aligned} \tag{29}$$

The Aziz II+MBM results for the pressure and the compressibility are plotted in Figs. 10 and 11, respectively, in comparison with the experimental values. One can observe that there are slight differences between the theoretical and the experimental results, which are more evident in the pressure case. In fact, these discrepancies reflect the departure of the Aziz II+MBM total energies from the experimental values when the density increases. This small effect on the energy, which can be observed in Fig. 9, is enlarged when the derivative magnitudes of the energy as $P(\rho)$ or $\kappa(\rho)$ are calculated.

IV. DISCUSSION

The properties of bulk liquid ^{4}He have been investigated by means of the diffusion Monte Carlo (DMC) method. It has been proved that the extension of the DMC algorithm up to second order (QDMC) allows for the possibility of calculating the energy without the extrapolation to $\Delta t=0$, required in the linear DMC code. We have applied the QDMC method in order to perform a comparative analysis between the Aziz and the Aziz II two-body potentials. The calculations have been extended to a wide range of densities in order to contrast the theoretical predictions on the equation of state provided by the two Aziz potentials. The results unambiguously demonstrate that the new Aziz potential gives better results than the old one, especially when the dependence of the pressure and the compressibility on the density is considered. In particular, the Aziz II results for $P(\rho)$ and $\kappa(\rho)$ are indistinguishable from the experimental values. However, the results for the energy are below the experimental determinations. This difference could suggest the presence of three-body interactions in He.

We have performed a Rayleigh-Schrödinger perturbative estimation of the three-body potential energy using two different models. The results obtained have shown that neither the triple-dipole potential of Axilrod-Teller nor the Bruch-McGee potential, which includes the exchange interaction at short distances, improve the equation of state given by the Aziz II potential. To make the three-body correction compatible with the experimental results a simple change in the parameters entering into

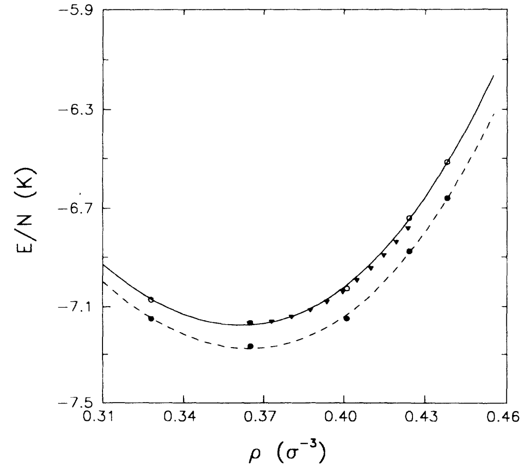

FIG. 9. Equation of state of liquid ^{4}He. The circles are the QDMC results with the Aziz II+MBM potentials; the solid line is a fit to these energies. The solid circles and the dashed line correspond to the calculation with the Aziz II potential. The solid triangles are the experimental values form Ref. 19. The error bars are smaller than the size of the symbols.

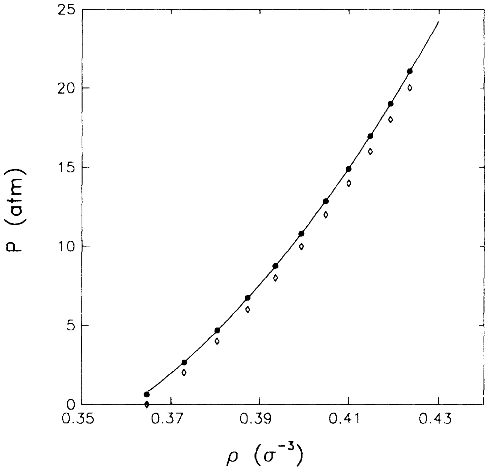

FIG. 10. Pressure of liquid ^{4}He as a function of the density. The solid circles are the Aziz II+MBM results and the diamonds are the experimental values from the equation of state (20). The solid line is a numerical fit to the data. The error bars are smaller than the size of the symbols.

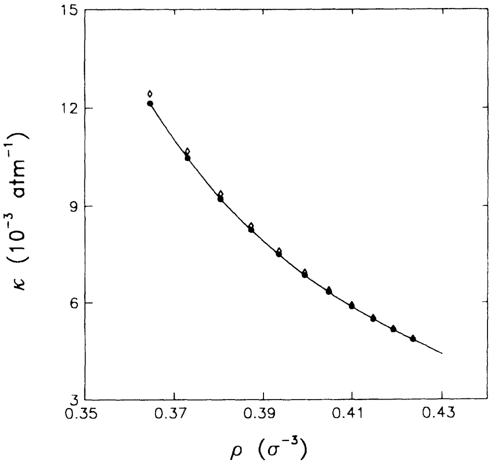

FIG. 11. Isothermal compressibility of liquid ^{4}He as a function of the density. The same notation as in Fig. 10.

the BM potential has been examined (MBM potential). The Aziz II+MBM model provides a good description of the equation of state $(E/N)(\rho)$, but the results for $P(\rho)$ and $\kappa(\rho)$ worsen with respect to the ones calculated with the Aziz II only. On the other hand, we would point out that the Aziz II results for the energy are shifted with respect to the experiment in a constant value for all the densities. This fact explains the excellent description of $P(\rho)$ and $\kappa(\rho)$ given by the new Aziz potential. The conclusion is that to account for the experimental energies, a constant value for $\langle V_3 \rangle$ would be required, although from the theoretical point of view it seems more plausible a correction which becomes larger when the density increases.

Concerning other properties as the radial distribution function or the momentum distribution, no significant differences between the results given by the two Aziz potentials are observed. Overall, the agreement between the QDMC results and the experiment is quite satisfactory. Finally, we would remark that the accuracy of the Aziz II potential in describing the bulk ^{4}He liquid phase makes it recommendable for future calculations of the solid phase or films, especially when the derivative magnitudes of the energy are among the main objectives.

ACKNOWLEDGMENTS

This work has been supported in part by DGICYT (Spain) Grant Nos. PB92-0761, PB90-06131, and TIC-0299/1989. Most of the simulations were performed on a multiprocessor CM2 from Thinking Machines of the CEPBA (Centre Europeu de Paral.lelisme de Barcelona).

APPENDIX A: TWO- AND THREE-BODY POTENTIALS

The form of the HFDHE2 (Aziz) potential[4] is

$$V(r)=\varepsilon\left[A\exp(-\alpha x)-F(x)\sum_{j=0}^{2}(C_{2j+6}/x^{2j+6})\right], \tag{A1}$$

where

$$F(x)=\begin{cases}\exp\left[-\left(\dfrac{D}{x}-1\right)^2\right], & x<D\\ 1, \quad x\geq D\end{cases} \tag{A2}$$

with

$$x=\frac{r}{r_m}. \tag{A3}$$

The values of the parameters for the Aziz potential are

$$\begin{aligned}&\varepsilon=10.8\ \text{K},\quad C_6=1.373\,241\,2\,,\\&r_m=2.9673\ \text{Å},\quad C_8=0.425\,378\,5\,,\\&D=1.241\,314\,,\quad C_{10}=0.1781\,,\\&\alpha=13.353\,384\quad A=0.544\,850\,4\times10^{6}\,.\end{aligned} \tag{A4}$$

The HFD-B(HE) (Aziz II) potential,[9] which is quite similar in form to the Aziz potential, is given by

$$V(r)=\varepsilon\left[A\exp(-\alpha x+\beta x^2)-F(x)\sum_{j=0}^{2}(C_{2j+6}/x^{2j+6})\right], \tag{A5}$$

where the function $F(x)$ and x are formally the same as in the Aziz potential [Eqs. (A2) and (A3)]. The values of the parameters for the Aziz II potential are

$$\begin{aligned}&\varepsilon=10.948\ \text{K},\quad C_6=1.367\,452\,14\,,\\&r_m=2.963\ \text{Å},\quad C_8=-0.421\,238\,07\,,\\&D=1.4826,\quad C_{10}=0.174\,733\,18\,,\\&\alpha=10.433\,295\,37,\quad A=1.844\,310\,1\times10^{5}\,,\\&\beta=-2.279\,651\,05\,.\end{aligned} \tag{A6}$$

The models for the three-body interactions we have used are those given by the Axilrod-Teller[30] (AT) and Brunch-McGee[32] (BM) potentials. The form of the AT potential is

$$V_3(r_{12},r_{13},r_{23})=\frac{\nu(1+3\cos\phi_1\cos\phi_2\cos\phi_3)}{r_{12}^3 r_{13}^3 r_{23}^3}, \tag{A7}$$

where ϕ_1, ϕ_2, and ϕ_3 are the interior angles of the triangle formed by the three atoms. We use the Leonard's helium value $\nu=0.327K\sigma^9$ (Ref. 35), assuming the radial distances r_{ij} in σ unities.

The BM potential is given by

$$\begin{aligned}V_3(r_{12},r_{13},r_{23})=&\left[\frac{\nu}{r_{12}^3 r_{13}^3 r_{23}^3}\right.\\&\left.-A\exp[-\alpha(r_{12}+r_{13}+r_{23})]\right]\\&\times(1+3\cos\phi_1\cos\phi_2\cos\phi_3)\,.\end{aligned} \tag{A8}$$

The values for the two new parameters appearing in the BM potential are

$$A=9\,676\,545.53\ \text{K},\quad \alpha=4.948\sigma^{-1}\,. \tag{A9}$$

APPENDIX B: TRIAL FUNCTIONS

In this appendix we give the explicit forms of the trial functions used as importance sampling in the QDMC calculations as well as the values of the parameters involved. The first one is the well-known McMillan two-body trial function[36]

$$\psi_{J1}=\prod_{i<j}\exp\left[-\frac{1}{2}\left(\frac{b}{r_{ij}}\right)^5\right]. \tag{B1}$$

We have taken the value $b=1.20\sigma$, which optimizes the VMC energy at the experimental equilibrium density.

Most of the present work has been carried out using the Reatto two-body function[37]

$$\psi_{J2}=\prod_{i<j}\exp\left\{-\frac{1}{2}\left[\frac{b}{r_{ij}}\right]^5-\frac{L}{2}\exp\left[-\left[\frac{r_{ij}-\lambda}{\Lambda}\right]^2\right]\right\}, \quad \text{(B2)}$$

with $L=0.2$, $\lambda=2.0\sigma$, $\Lambda=0.6\sigma$, and $b=1.20\sigma$. These values, optimal at the experimental equilibrium density, have also been used for the other densities.

The third trial function, which was proposed by Schmidt *et al.*,[38] contains two- and three-body correlations. It is explicitly given by

$$\psi_{JT}=\psi_{J1}\exp\left[-\frac{1}{4}\lambda\sum_{k}\mathbf{G}_k\cdot\mathbf{G}_k+\frac{1}{2}\lambda\sum_{i<j}\xi^2(r_{ij})r_{ij}^2\right], \quad \text{(B3)}$$

where

$$\mathbf{G}_k=\sum_{l\neq k}\xi(r_{kl})\mathbf{r}_{kl} \quad \text{(B4)}$$

and

$$\xi(r)=\exp\left[-\left[\frac{r-r_t}{r_\omega}\right]^2\right]. \quad \text{(B5)}$$

The values for the triplet parameters, roughly optimal at the equilibrium density, are $\lambda=-1.08\sigma^{-2}$, $r_t=0.80\sigma$, and $r_\omega=0.41\sigma$.

---

[1] S. Rosati and M. Viviani, in *First International Course on Condensed Matter,* edited by D. Prosperi *et al.* (World Scientific, Singapore, 1988).

[2] A. Fabrocini and S. Fantoni, in *First International Course on Condensed Matter* (Ref. 1).

[3] A modern review of Monte Carlo methods may be found in *Monte Carlo Methods in Theoretical Physics,* edited by S. Caracciolo and A. Fabrocini (ETS Editrice, Pisa, 1991).

[4] R. A. Aziz, V. P. S. Nain, J. S. Carley, W. L. Taylor, and G. T. McConville, J. Chem. Phys. **70**, 4330 (1979).

[5] M. H. Kalos, M. A. Lee, P. A. Whitlock, and G. V. Chester, Phys. Rev. B **24**, 115 (1981).

[6] V. R. Pandharipande, J. G. Zabolitsky, S. C. Pieper, R. B. Wiringa, and V. Helmbrehct, Phys. Rev. Lett. **50**, 1676 (1983).

[7] S. A. Chin and E. Krotscheck, Phys. Rev. B **45**, 852 (1992).

[8] J. L. Vallés and K. E. Schmidt, Phys. Rev. B **38**, 2879 (1988).

[9] R. A. Aziz, F. R. W. McCourt, and C. C. K. Wong, Mol. Phys. **61**, 1487 (1987).

[10] D. M. Ceperley and H. J. Partridge, J. Chem. Phys. **84**, 820 (1986).

[11] D. M. Ceperley and M. H. Kalos, in *Monte Carlo Methods in Statistical Physics,* edited by K. Binder (Springer, Berlin, 1979).

[12] M. H. Kalos, D. Levesque, and L. Verlet, Phys. Rev. A **9**, 2178 (1974).

[13] R. Guardiola, in *First International Course on Condensed Matter* (Ref. 1).

[14] P. J. Reynolds, D. M. Ceperley, B. J. Alder, and W. A. Lester, J. Chem. Phys. **77**, 5593 (1982).

[15] D. M. Ceperley and B. J. Alder, Phys. Rev. B **36**, 2092 (1987).

[16] S. A. Chin, Phys. Rev. B **42**, 6991 (1990).

[17] R. Barnett, P. Reynolds, and W. Lester, Jr., J. Comput. Phys. **96**, 258 (1991).

[18] S. Zhang and M. H. Kalos, J. Stat. Phys. **70**, 515 (1993).

[19] R. De Bruyn Ouboter and C. N. Yang, Physica B **44**, 127 (1987).

[20] J. Boronat, A. Fabrocini, and A. Polls, Phys. Rev. B **39**, 2700 (1989).

[21] S. Stringari and J. Treiner, Phys. Rev. B **36**, 8369 (1987).

[22] P. A. Whitlock, D. M. Ceperley, G. V. Chester, and M. H. Kalos, Phys. Rev. B **19**, 5598 (1979).

[23] E. C. Svensson, V. F. Sears, A. D. B. Woods, and P. Martel, Phys. Rev. B **21**, 3638 (1980).

[24] F. H. Wirth and R. B. Hallock, Phys. Rev. B **35**, 89 (1987).

[25] G. Galglione, G. L. Masserini, and L. Reatto, Phys. Rev. B **23**, 1129 (1981).

[26] E. Manousakis, V. R. Pandharipande, and Q. N. Usmani, Phys. Rev. B **31**, 7022 (1985); **43**, 13 587 (1991).

[27] P. Whitlock and R. M. Panoff, Can. J. Phys. **65**, 1409 (1987).

[28] H. A. Mook, Phys. Rev. Lett. **51**, 1454 (1983).

[29] J. Gavoret and Ph. Nozieres, Ann. Phys. (N.Y.) **28**, 349 (1964).

[30] B. M. Axilrod and E. Teller, J. Chem. Phys. **11**, 299 (1943).

[31] R. D. Murphy and J. A. Barker, Phys. Rev. A **3**, 1037 (1971).

[32] L. W. Bruch and I. J. McGee, J. Chem. Phys. **59**, 409 (1973).

[33] O. A. Novaro and V. Beltran-Lopez, J. Chem. Phys. **56**, 815 (1972).

[34] P. Loubeyre, Phys. Rev. Lett. **58**, 1857 (1987).

[35] P. J. Leonard, M. Sc. thesis, University of Melbourne, 1968 (unpublished); cited in Ref. 31.

[36] W. L. McMillan, Phys. Rev. **138**, 442 (1965).

[37] L. Reatto, Nucl. Phys. **A328**, 253 (1979).

[38] K. Schmidt, M. H. Kalos, M. A. Lee, and G. V. Chester, Phys. Rev. Lett. **45**, 573 (1980).